Amorphous-to-crystalline transformation of $Fe_{82}B_{12}Si_6$

Hang Nam Ok* and A. H. Morrish
Department of Physics, University of Manitoba, Winnipeg, Manitoba, Canada R3T 2N2
(Received 12 May 1980)

The transformation from the as-quenched amorphous to the crystalline state of $Fe_{82}B_{12}Si_6$ (METGLAS® 2605S) has been investigated by Mössbauer spectroscopy, x-ray diffraction, and density measurements. The first step of the transformation is found to be structural relaxation during which atomic rearrangements towards a more stable amorphous state take place. In the second step, crystalline Fe-9 at.% Si alloy precipitates out until the metastable amorphous phase $Fe_{77}B_{18}Si_5$ is formed. The final products of crystallization are found to be Fe-9 at.% Si alloy and Fe_2B. The distribution of the Si atoms amongst the bcc lattice points of the precipitated Fe-Si alloy is random at low annealing temperatures T_A. However, at higher T_A short-range ordering of Si atoms appears and increases with increasing T_A. During crystallization the Mössbauer recoil-free fraction of the ^{57}Fe nuclei increased by 39%. The density also increased from 7.28 to 7.49 g/cm^3. These two observations imply that the Fe atoms are more firmly bound in the crystalline than in the amorphous state. During structural relaxation an increase of atomic ordering was observed; this is proposed as the origin of the small increase in the magnetic hyperfine field with increasing T_A before the onset of crystallization.

I. INTRODUCTION

Recently, the amorphous to crystalline transformation of metallic glasses has drawn considerable attention, and some interesting results have been obtained from Mössbauer measurements. The most intensively studied glasses are the binary ones, $Fe_{1-x}B_x$ ($x < 0.25$), especially $Fe_{80}B_{20}$, because they have the simplest possible forms. Two types of crystallization process have been observed for these simple binary alloys. The first type[1–3] has been observed for amorphous Fe-B alloys with a B concentration of less than 16 at.%, and consists of two steps. The first step of crystallization is a precipitation of α-Fe until the composition of the remaining glass transforms into a Fe_3B metastable compound that decomposes at higher temperatures into α-Fe and Fe_2B. The second type[1,3,4] of crystallization has been observed for amorphous Fe-B alloys with a B concentration of more than about 16 at.% and consists of a single step; the crystallization takes place by the eutectic type of reaction. The two crystalline phases, α-Fe and Fe_3B are produced from the very beginning of crystallization, and the α-Fe to Fe_3B ratio is constant throughout the transformation.

Another interesting result reported is the change in the Mössbauer recoil-free fraction in connection with the transition from the amorphous to crystalline state. According to Schaafsma and co-workers,[4] the recoil-free fraction of the ^{57}Fe nuclei in $Fe_{80}B_{20}$ was constant before the onset of crystallization but it increased by about 15% during crystallization. On the other hand, Schurer and Morrish[5] observed a slight increase of the ^{57}Fe recoil-free fraction in $Fe_{32}Ni_{36}Cr_{14}P_{12}B_6$ before crystallization set in, and suggested that structural relaxation resulting in a reversible configuration was responsible for the increase.

In the present paper the transformation of the ternary metallic glass $Fe_{82}B_{12}Si_6$ (METGLAS® 2605S) from the as-quenched amorphous to the crystalline state is followed with Mössbauer spectroscopy, x-ray diffraction, and density measurements. The amorphous to crystalline transformation depends on both the annealing time and the temperature.

II. EXPERIMENTAL

Amorphous $Fe_{82}B_{12}Si_6$ (METGLAS® 2605S) in the form of a ribbon 2.54 cm wide and 38 μm thick was obtained from the Allied Chemical Corp. The samples cut from the ribbon roll were placed between two stainless-steel plates (thickness 3.2 mm) and then annealed in a helium atmosphere in a furnace with a temperature stability of 1.5 °C. Various annealing temperatures ranging from 400 to 1200 K were used and the annealing time was fixed to be 20 min for each sample. The heating time to the annealing temperature was 15 min. Mössbauer spectra were collected with an Elscint constant acceleration spectrometer that had linewidths of 0.25 mm/s for the inner lines of a natural iron absorber 12.7 μm thick. A ^{57}Co source in Rh matrix was used throughout the experiments.

The x-ray diffraction patterns used for determining the radial distribution functions were obtained using a diffractometer (Mo $K\alpha$ radiation) equipped with a step-scanning mechanism. The intensity of the dif-

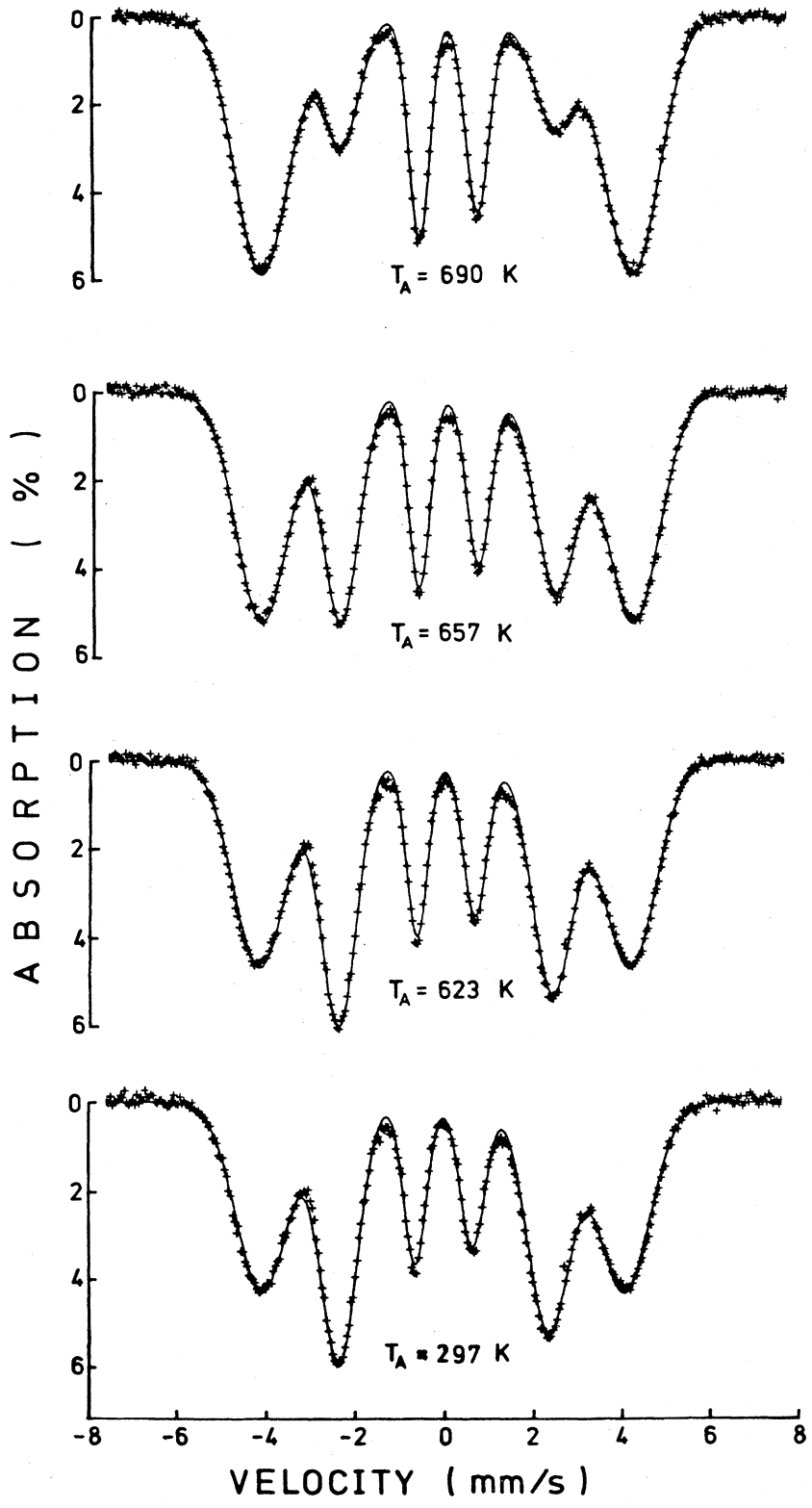

FIG. 1. Mössbauer spectra of amorphous $Fe_{82}B_{12}Si_6$ at room temperature after annealing at various temperatures T_A for 20 min.

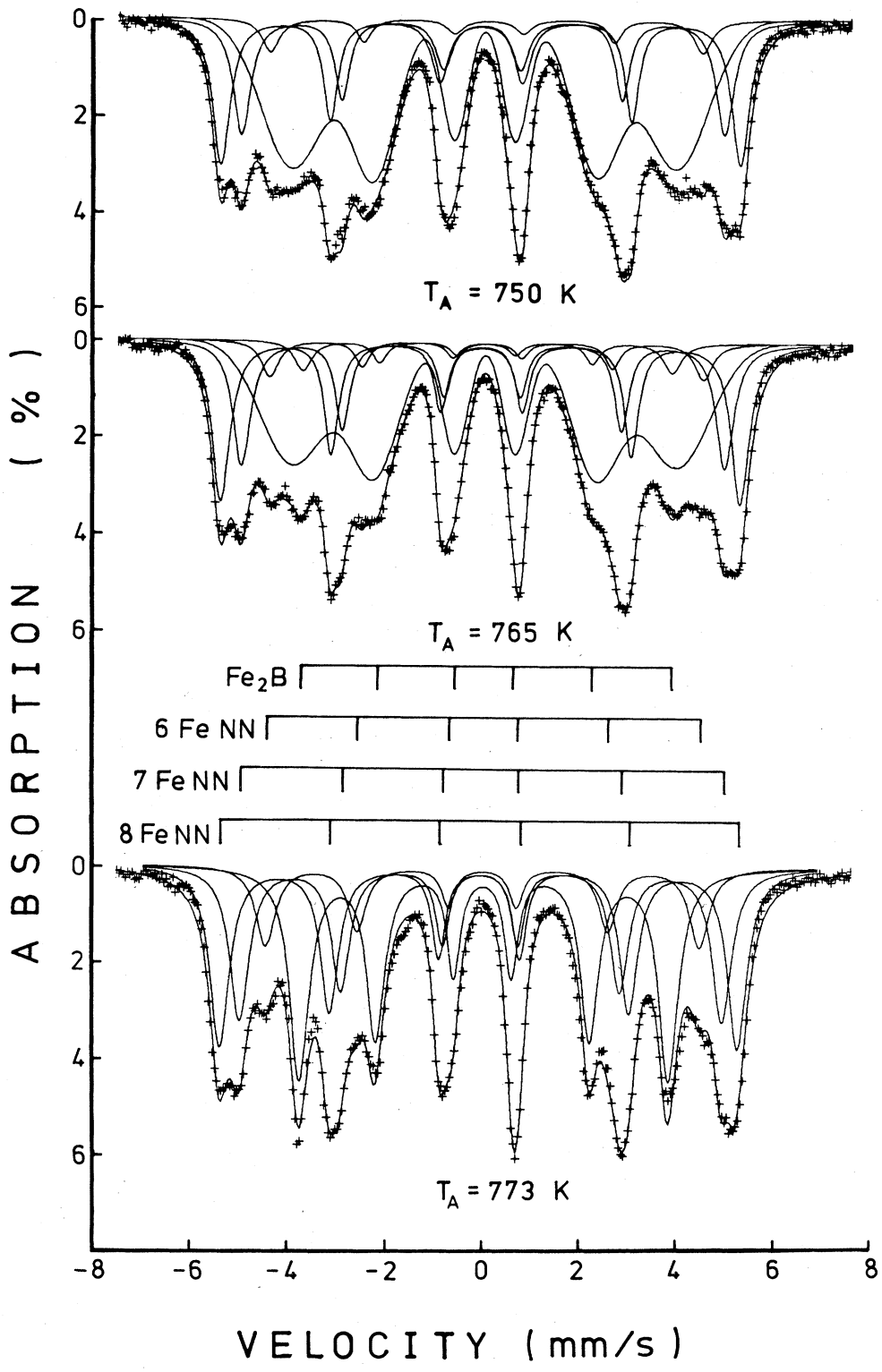

FIG. 2. Mössbauer spectra of $Fe_{82}B_{12}Si_6$ at room temperature after annealing at various temperatures T_A for 20 min.

fracted beam was measured with a scintillation counter and the contribution of $\frac{1}{2}\lambda$ was eliminated by a pulse-height analyzer. The diffraction patterns were recorded in a range of 2θ (θ is the Bragg angle) from 6 to 150°. In order to avoid the correction for the angular dependence of the absorption, the specimen was made thick enough (270 μm) by overlapping seven foils. Densities were determined by comparing the specimen weight in air and bromoform ($CHBr_3$, density equal to 2.865 g/cm^3) at room temperature.

III. RESULTS AND DISCUSSIONS

A. Crystallization products

Figure 1 shows typical examples of Mössbauer spectra for the samples annealed at temperatures below 700 K; these spectra consist of six well defined but broadened lines. However, as T_A is raised above 700 K, sharp lines of crystalline phases appear, as exhibited in Fig. 2. At $T_A = 773$ K, the amorphous sample is completely crystallized; Fig. 2 shows that the Mössbauer spectrum then consists of four sets of six-line patterns. Least-squares fitting has been carried out using Gaussian line shapes for the amorphous phase and Lorentzian line shapes for the crystalline phases. The reason why Gaussian line shapes were used instead of the usual Lorentzian line shapes was based on the result[6] that when the broadened absorption lines of amorphous solids were separated by an external magnetic field, Gaussian line shapes gave better fits. In the present analysis, lines symmetrically located in a pattern are assumed to have the same areas. Furthermore, the relative intensities of lines one, two, and three for each pattern were restricted to be the same for all four crystalline patterns. The results of the analyses for the four six-line patterns of the completely crystallized sample ($T_A = 773$ K) are shown in Table I. In order to identify the crystalline products, possible stable crystalline compounds and alloys[7–12] producible from $Fe_{82}B_{12}Si_6$ are listed in Table II. By comparing Table I with Table II, one can easily identify the first three crystalline patterns in Table I with the three Fe sites in Fe-Si alloy and the fourth crystalline pattern with Fe_2B. As can be

TABLE I. Magnetic hyperfine fields H_{hf}, isomer shifts δ, and quadrupole splittings ϵ, at room temperature for the four crystalline patterns of completely crystallized $Fe_{82}B_{12}Si_6$ annealed at 773 K. The isomer shifts are relative to iron metal. The quadrupole splittings have been calculated from the positions of the Mössbauer absorption lines using the expression $\epsilon = (v_6 - v_5 + v_1 - v_2)/2$, where v_i represents the position of the ith absorption line. The figures in parentheses are the probable errors.

H_{hf} (kOe)	δ (mm/s)	ϵ (mm/s)
331 (1)	0.02 (1)	−0.01 (1)
308 (1)	0.06 (1)	0.01 (1)
277 (1)	0.09 (1)	0.00 (1)
236 (1)	0.12 (1)	0.02 (1)

TABLE II. Crystal structure, name of sites, magnetic hyperfine field H_{hf}, and isomer shift δ, at room temperature of stable crystalline compounds and alloys that could conceivably be products of the amorphous-to-crystalline transformation of $Fe_{82}B_{12}Si_6$. The isomer shifts are relative to iron metal.

Crystals	Structure	Sites	H_{hf} (kOe)	δ (mm/s)	Ref.
α-Fe	bcc		330	0	a
Fe_3Si	DO_3	*A*	201	0.26	b
		D	310	0.08	
FeB	Orthorhombic		118	0.28	c
Fe_2B	Tetragonal		237	0.12	d
Fe_5SiB_2	Tetragonal	Fe(1)*a*	170	0.28	e
		Fe(1)*b*	198	0.28	
		Fe(2)	230	0.12	
Fe-8.6 at.% Si	bcc	8 Fe NN	331	0.02	f
		7 Fe NN	308	0.05	
		6 Fe NN	277	0.10	

[a]Reference 7.
[b]Reference 8.
[c]Reference 9.
[d]Reference 10.
[e]Reference 11.
[f]Reference 12.

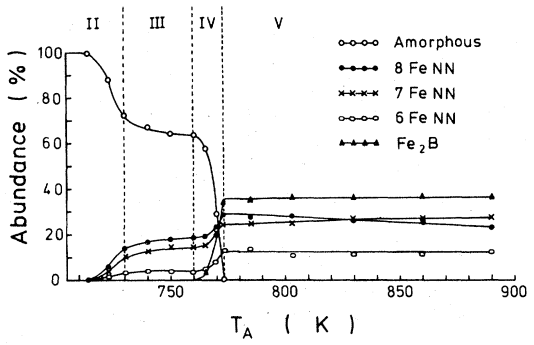

FIG. 3. Relative abundance of various phases or sites as a function of annealing temperature T_A.

seen in Figs. 2 and 3, only the Fe-Si alloy precipitates out below $T_A = 760$ K. However, above $T_A = 760$ K, both the Fe-Si alloy and Fe_2B appear. Note that no trace of crystalline Fe_3Si was detected in the Mössbauer spectra.

In order to estimate the Si concentration c in this precipitated Fe-Si alloy, Si atoms are assumed to be distributed randomly at bcc lattice sites. Then the probability for an iron atom to have l Fe nearest neighbors is given by

$$P(c,l) = \binom{8}{l}(1-c)^l c^{8-l} \tag{1}$$

and the results of this calculation are listed in Table III. Comparison of Table III with Fig. 4 shows that the intensity ratio corresponding to a Si concentration of 9 at.% is closest to the experimental values of the samples annealed below 760 K. Furthermore, x-ray diffraction patterns taken for both the precipitated Fe-Si alloy and pure α-Fe under the same experimental conditions show that the lattice parameter ratio of the precipitated Fe-Si alloy to α-Fe is 0.9975 ± 0.0001, which is the same as that found in Fe-9 at.% Si alloy.[13] The precipitation of the Fe-Si alloy from $Fe_{82}B_{12}Si_6$ differs somewhat from that observed in other amorphous materials, namely, the α-Fe precipitation in $Fe_{1-x}B_x$ and $Fe_{84}B_{16-x}C_x$ amorphous alloys.[2,14]

B. Structural relaxation

In order to study the atomic rearrangements before crystallization sets in at about 700 K, the temperature for the onset of bulk crystallization was first determined. Since the six-line patterns of the crystalline Fe-9% Si alloy overlap with that of the amorphous phase at room temperature, Mössbauer spectra were taken at 470 K for three samples annealed at 690, 714, and 727 K, respectively. As shown in Fig. 5, the sample annealed at 727 K is partially crystallized and a trace of the crystalline phase is detected in the sample annealed at 714 K.

Figure 6 shows x-ray diffraction patterns taken for the as-quenched sample and two samples annealed at 690 and 714 K, respectively. Again, a small crystalline peak is seen on the top of the broad amorphous line for the sample annealed at 714 K, whereas there is no trace of a crystalline phase for the sample annealed at 690 K. However, the linewidth of the broad amorphous peak of the sample annealed at 690 K is slightly narrower than that of the corresponding peak of the as-quenched sample, implying the occurrence of atomic rearrangement during annealing.

In order to pursue this point further, the usual Fourier-inversion analysis[15] has been carried out for the x-ray diffraction patterns collected from $2\theta = 6$ to 150° for both the as-quenched sample and the sample annealed at 690 K. Figure 7 shows the radial distribution functions: $4\pi r^2\rho$, where

$$4\pi r^2\rho = 4\pi r^2\rho_0 + (2r/\pi)\int_0^{K_{\max}} K[I(K)-1]\sin(Kr)\,dK \ , \tag{2}$$

ρ_0 is the average atomic density, and $K = 4\pi\sin\theta/\lambda$. The interference function $I(K)$ has been calculated using the expression

$$I(K) = \frac{I_{\text{obs}} - \langle|f|^2\rangle}{|\langle f\rangle|^2} + 1 \ , \tag{3}$$

where I_{obs} is the observed intensity in electron units corrected for background and polarization. The atomic scattering factors[16] f computed from numeri-

TABLE III. Normalized relative occupation probabilities in percent for a random distribution of Si. Here c denotes the concentration of Si and l the number of Fe nearest neighbors for a particular iron atom.

l \ c	7%	8%	9%	10%	11%
8	57	52	48	45	41
7	34	36	38	40	41
6	9	11	13	15	18

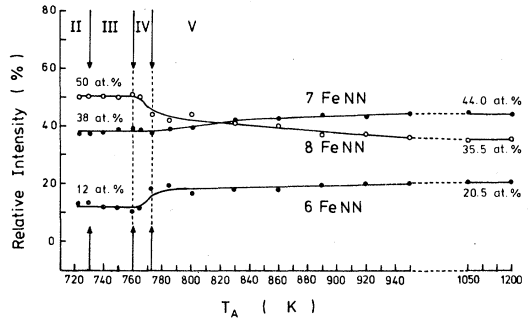

FIG. 4. Relative intensity of various sites in the precipitated Fe-Si alloy as a function of annealing temperature T_A.

cal Hartree-Fock wave functions were used. In Fig. 7, the peaks of the radial distribution function become sharper for the sample annealed at 690 K than for the as-quenched sample, implying atomic rearrangements toward more ordering with annealing. This increase of ordering may be the origin of the tendency for the magnetic hyperfine field to increase with increasing annealing temperature up to $T_A = 700$ K, as shown in Fig. 8(a); the apparent reason is that the long-range exchange interactions responsible for the ferromagnetism of the amorphous $Fe_{82}B_{12}Si_6$ are strengthened by the increase of atomic ordering.

Figure 8(b) shows the relative values of the Mössbauer recoil-free fraction at room temperature as a function of annealing temperature. The recoil-free fraction or f_R factor can be expressed as

$$f_R = \exp(-4\pi\langle x^2\rangle/\lambda^2) \ , \tag{4}$$

where λ is the γ-ray wavelength and $\langle x^2\rangle$ is the mean-square vibrational amplitude of the nucleus in the propagation direction of the γ ray. Thus, the f_R factor value reflects the binding state of the lattice. As shown in Fig. 8(b), the f_R factor, or the total area of the Mössbauer absorption lines, of amorphous $Fe_{82}B_{12}Si_6$ increases slowly during structural relaxation below $T_A = 700$ K; the little depression near $T_A = 690$ K seems to come from saturation effects of the absorption lines 1 and 6 because a much larger part of the total absorption area is concentrated on the two lines 1 and 6 at $T_A = 690$ K than at any other temperatures as shown in Fig. 1. This increase of f_R factor before the onset of crystallization seems to indicate that structural relaxation results in a more stable atomic configuration, to be compared to the reversible changes in $Fe_{32}Ni_{36}^{0}Cr_{14}P_{12}B_6$ glass.[5]

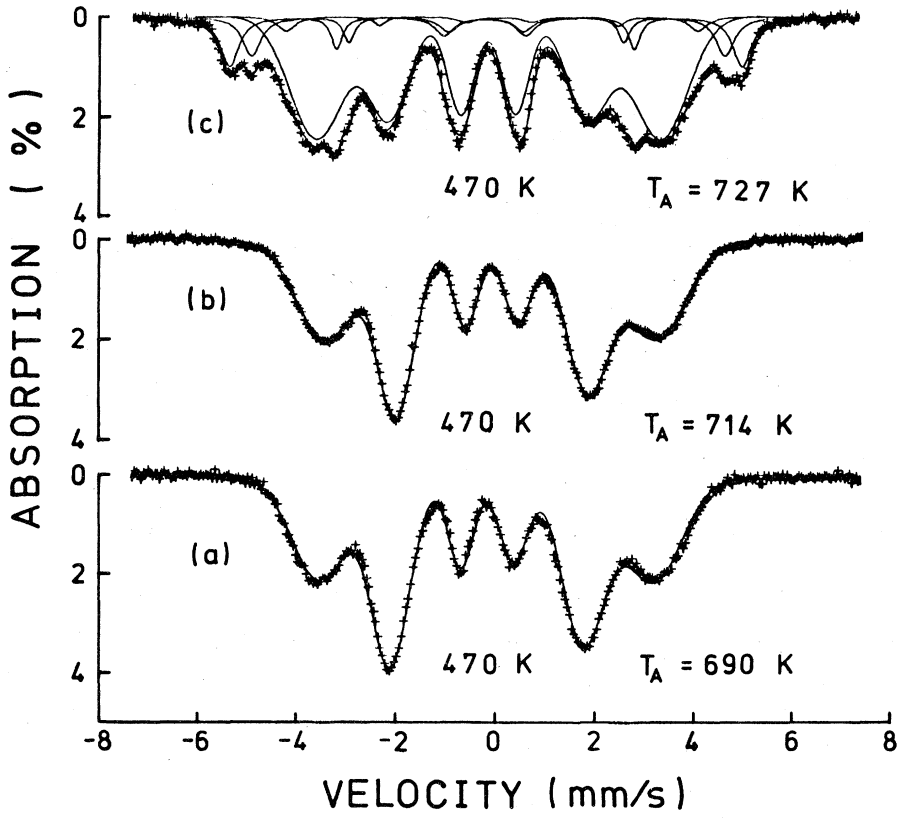

FIG. 5. Mössbauer spectra of $Fe_{82}B_{12}Si_6$ at 470 K after annealing at (a) 690, (b) 714, and (c) 727 K for 20 min.

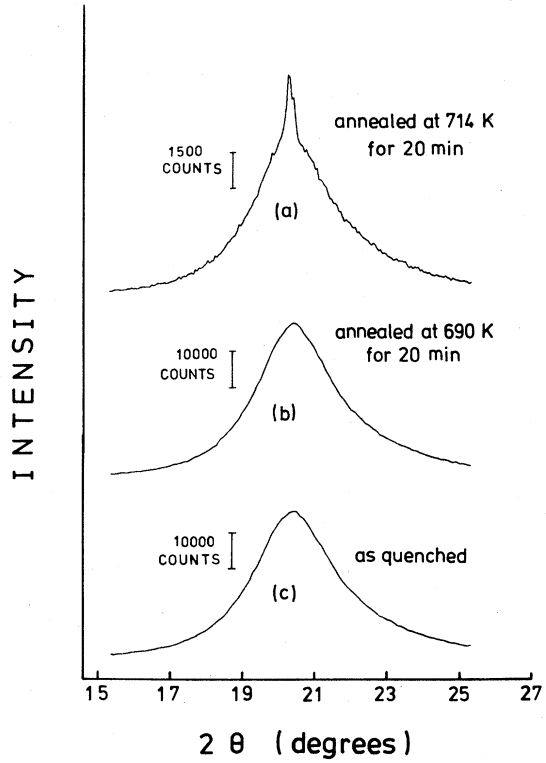

FIG. 6. X-ray diffraction patterns of $Fe_{82}B_{12}Si_6$ at room temperature after annealing at 714, 690, and 297 K.

C. Initial crystallization

Crystallization proceeds slowly as the annealing temperature T_A increases from 700 to 714 K and then the crystalline Fe-9 at.% Si alloy precipitates out rapidly above $T_A = 714$ K as shown in the region II of Fig. 3. At the same time, the recoil-free fraction increases slowly at first and then jumps up to a value

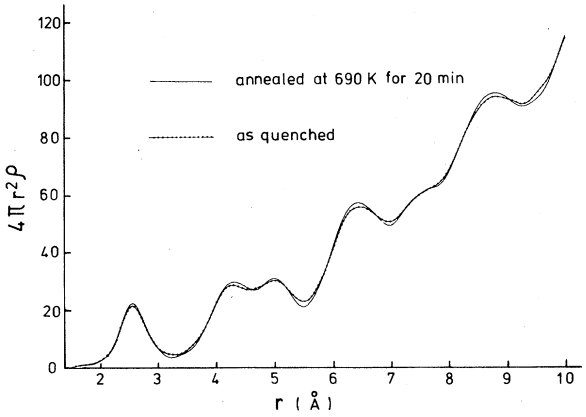

FIG. 7. Radial distribution functions ($4\pi r^2\rho$) of as-quenched $Fe_{82}B_{12}Si_6$ sample and after annealing at 690 K.

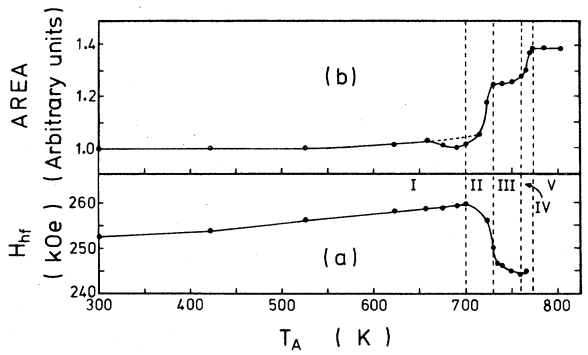

FIG. 8. (a) The magnetic hyperfine field H_{hf} of the amorphous phase and (b) the relative recoil-free fraction at room temperature of $Fe_{82}B_{12}Si_6$ after annealing at various temperatures T_A for 20 min.

25% higher than that of the as-quenched amorphous phase as indicated in the region II of Fig. 8. The implication is that the Fe atoms, on the average, are more firmly bound in the crystalline than in the amorphous state. As crystallization proceeds, the magnetic hyperfine field of the remaining amorphous phase decreases quickly as shown in the region II of Fig. 8(a). This decrease can be related to the Fe concentration as follows. Since the precipitated crystalline Fe-Si alloy has a larger Fe concentration (91 at.%) than the original amorphous $Fe_{82}B_{12}Si_6$, the increased precipitation of the Fe-Si alloy will leave an amorphous phase of smaller iron concentration, and thereby weakening the exchange interaction.

D. Metastable amorphous state

When the annealing temperature was increased above $T_A = 730$ K, crystallization proceeded very slowly as shown in the region III of Fig. 3. Similar stationary behaviors are seen in the f_R factor and the magnetic hyperfine field of the remaining amorphous phase in Fig. 8. In other words, a metastable state has been formed. The composition of this metastable amorphous state can be estimated using the crystallization equation

$$Fe_{82}B_{12}Si_6 \rightarrow x\,Fe_{91}Si_9 + Fe_{82-91x}B_{12}Si_{6-9x} \ , \qquad (5)$$

where the first term represents the precipitated crystalline Fe-9 at.% Si alloy and the second one the remaining amorphous phase. By using the stationary value of 63% as the relative abundance of the amorphous phase, one can get the following relation:

$$\frac{82-91x}{91x} = \frac{63}{37}$$

from which it follows that $x = 0.333$. The composition of the metastable amorphous phase is immedi-

TABLE IV. Density values of the various $Fe_{82}B_{12}Si_6$ samples. The figures in parentheses are the probable errors.

Samples	Density (g/cm^3)
As quenched	7.28 (1)
Annealed at 690 K	7.29 (1)
Annealed at 720 K	7.30 (1)
Completely crystallized	7.49 (1)

ately obtained from Eq. (5), viz.,

$$Fe:B:Si::82-91x:12:6-9x::77:18:5 \ .$$

The transition-metal to metalloid ratio is 77:23 for the metastable amorphous phase. It is interesting to note that this ratio is very close to the metal-metalloid ratio of 75:25 found for the metastable crystalline compounds[1-4,14] Fe_3B and $Fe_3(B_{1-y}C_y)$ appearing in the process of crystallization of the amorphous Fe-B alloys and $Fe_{84}B_{16-x}C_x$, respectively. Finally, it should be mentioned that the magnetic hyperfine field of the metastable amorphous phase

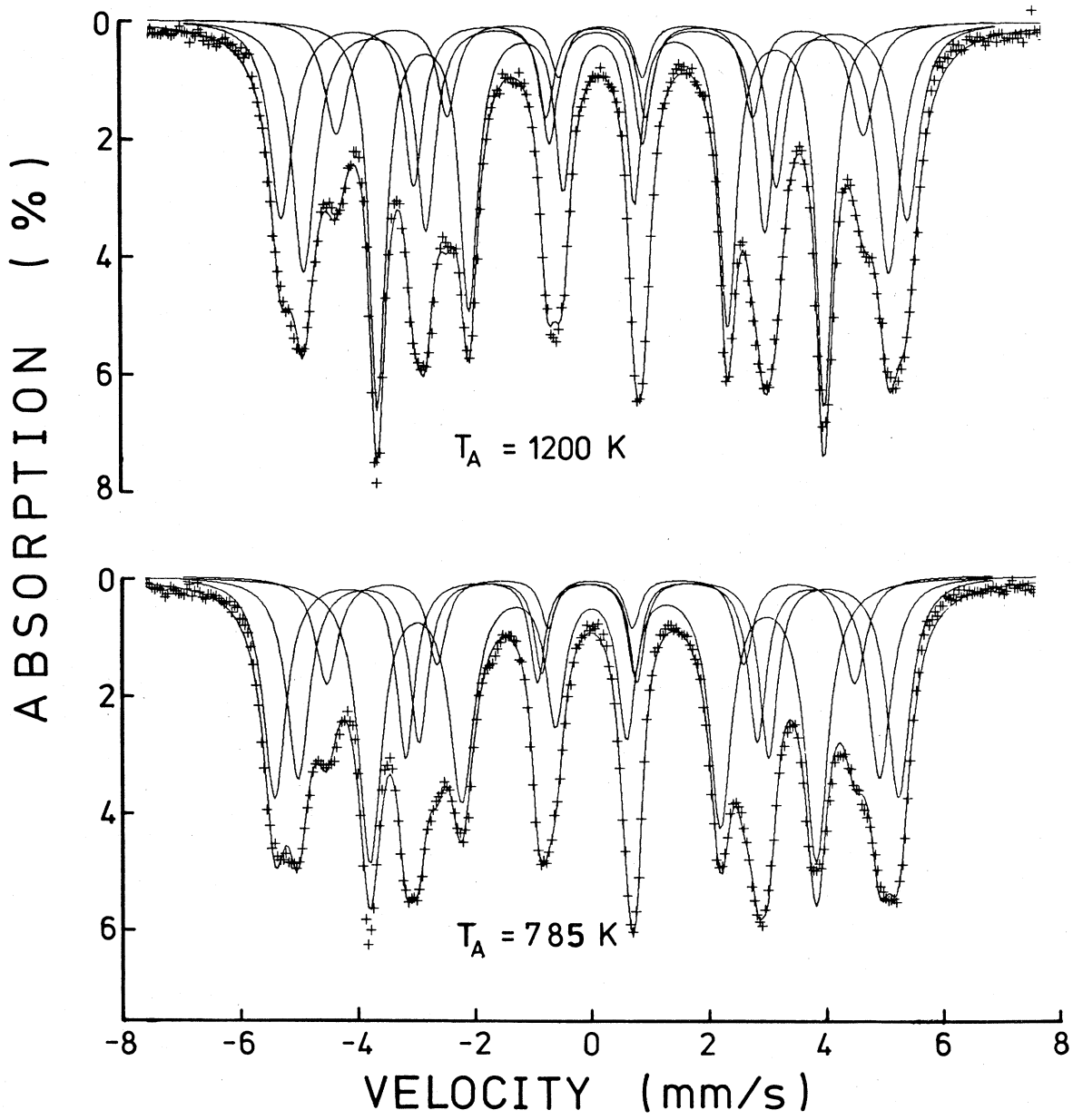

FIG. 9. Mössbauer spectra of crystallized $Fe_{82}B_{12}Si_6$ at room temperature after annealing at 785 and 1200 K for 20 min.

$Fe_{77}B_{18}Si_5$ is 244 kOe, which is considerably lower than 253 kOe of the as-quenched amorphous phase of $Fe_{82}B_{12}Si_6$, because there is a large difference in the Fe concentration.

E. Final crystallization

When the annealing temperature T_A was raised above 760 K, crystallization proceeded rapidly and was completed at about 773 K as shown in the region IV of Fig. 3. During this final crystallization, a new crystalline phase, Fe_2B, appeared and grew quickly to become the most abundant component. During the same time, the recoil-free fraction rose to a value 39% higher than that of the original as-quenched amorphous phase, as shown in the region IV of Fig. 8. This result is consistent with the large increase of density upon completion of crystallization as can be seen in Table IV.

F. Ordering in the crystalline phase

Figure 9 shows how the Mössbauer spectra change with increasing annealing temperature even after completion of crystallization. Comparison of Fig. 9 with Fig. 2 establishes that the intensities of the 8 Fe nearest-neighbor (NN) lines decrease relative to those of the 7 Fe NN lines as T_A increases. X-ray-diffraction patterns show that no other lines appear above $T_A = 773$ K other than those of bcc Fe-Si and tetragonal Fe_2B. Furthermore, the amount of Fe_2B remains unchanged during this transition, as can be seen in the region V of Fig. 3, and the solubility of B in the bcc Fe lattice is extremely small (only 0.0002 wt.% at 983 K).[17] Therefore, it may be concluded that atomic rearrangements have taken place inside the bcc lattice of the precipitated Fe-Si alloy. In order to concentrate attention on the bcc Fe-Si alloy, relative intensities among Fe-Si lines are calculated and shown in Fig. 4. The relative intensity ratio for 8 Fe NN:7 Fe NN:6 Fe NN at low T_A is 50:38:12, which corresponds to the random distribution of Si atoms among the bcc lattice points, as shown in Sec. A. However, as T_A increases, the ratio deviates from that for a random distribution of Si and finally reaches the value of 36:44:21. Since no superstructure lines are observed in the x-ray-diffraction pattern of the sample annealed at 1200 K, it is suggested that the atomic rearrangements inside the precipitated Fe-Si alloy are of short-range order.

IV. CONCLUSIONS

The transformation from the as-quenched amorphous to the crystalline state of $Fe_{82}B_{12}Si_6$ can be divided into the following five regions depending on the annealing temperatures T_A.

(i) In the temperature region, $T_A < 700$ K, the atoms rearrange to become more ordered with increasing T_A without bulk crystallization occurring. This increase of atomic ordering is proposed as the principal origin for the tendency of the magnetic hyperfine field to increase with increasing T_A. This model also can account for a similar increase in the magnetic hyperfine field before the onset of crystallization reported for $Fe_{75}P_{15}C_{10}$,[18] $Fe_{40}Ni_{38}Mo_4B_{18}$,[19] $Fe_{78}B_{12}Si_{10}$,[20] and $Fe_{40}Ni_{40}P_{14}B_6$ (Ref. 21) annealed at 600, 650, 710, and 545 K, respectively. The slow increase in the Mössbauer recoil-free fraction with increasing T_A suggests that structural relaxation leads to a more stable atomic configuration, which has also been observed for the $Fe_{32}Ni_{36}Cr_{14}P_{12}B_6$ alloy.[5]

(ii) In the temperature region, $700 < T_A < 730$ K, bulk crystallization develops with the precipitation of crystalline Fe-9 at.% Si alloy. During this process, the recoil-free fraction increases by 25%, reflecting increased binding. However, the magnetic hyperfine field of the remaining amorphous phase decreases rapidly with increasing T_A. This decrease can be understood on the basis of the decreased iron concentration that results from the precipitation of the higher Fe-concentration $Fe_{91}Si_9$ alloy.

(iii) In the temperature region $730 < T_A < 760$ K, crystallization proceeds very slowly and a metastable amorphous state is formed. The composition of this amorphous phase is found to be $Fe_{77}B_{18}Si_5$ whose metal-to-metalloid ratio is similar to the 75:25 ratio for the metastable crystalline phases Fe_3B and $Fe_3(B_{1-y}C_y)$ appearing in the process of crystallization of the amorphous Fe-B alloys and $Fe_{84}B_{16-x}C_x$, respectively.

(iv) In the temperature region, $760 < T_A < 773$ K, crystallization is completed. During this final crystallization, a new crystalline phase Fe_2B appears and the recoil-free fraction rises to a value 39% higher than that of the original as-quenched amorphous phase. The increase of binding upon crystallization is also manifested in the increase of density from 7.28 to 7.49 g/cm^3.

(v) As T_A is increased above 760 K, the distribution of Si atoms amongst bcc Fe-Si lattice points changes from random to short-range ordering.

ACKNOWLEDGMENT

Financial support was provided by the Natural Science and Research Council of Canada.

*On leave from the Dept. of Phys., Yonsei Univ., Seoul, Korea.
[1]K. Fukamichi, M. Kikuchi, S. Arakawa, and T. Masumoto, Solid State Commun. 23, 955 (1977).
[2]T. Kemeny, I. Vincze, and B. Fogarassy, Phys. Rev. B 20, 476 (1979).
[3]T. Tarnoczi, I. Nagy, C. Hargitai, and M. Hosso, IEEE Trans. Magn. 14, 1025 (1978).
[4]A. S. Schaafsma, H. Snijders, and F. van der Woude, Phys. Rev. B 20, 4423 (1979).
[5]P. J. Schurer and A. H. Morrish (unpublished).
[6]P. J. Schurer and A. H. Morrish, Solid State Commun. 28, 819 (1978).
[7]R. S. Preston, S. S. Hanna, and J. Heberle, Phys. Rev. 128, 2207 (1962).
[8]I. Vincze and I. A. Campbell, Solid State Commun. 14, 795 (1974).
[9]J. D. Cooper, T. C. Gibb, N. N. Greenwood, and R. V. Parish, Trans. Faraday Soc. 60, 2097 (1964).
[10]L. Takács, M. C. Cadeville, and I. Vincze, J. Phys. F 5, 800 (1975).
[11]T. Ericsson, L. Häggström, and R. Wäppling, Phys. Scr. 17, 83 (1978).
[12]L. Häggström, L. Grånäs, R. Wäppling, and S. Devanarayanan, Phys. Scr. 7, 125 (1973).
[13]M. C. Farquhar, H. Lipson, and A. R. Weill, J. Iron Steel Inst. London 152, 457 (1945).
[14]J. Balogh, I. Dezsi, B. Fogarassy, L. Gránàssy, D. L. Nagy, I. Vincze, and S. Arajs, J. Phys. (Paris) Colloq. 41, C1-253 (1980).
[15]C. S. Cargill II, Solid State Phys. 30, 227 (1975).
[16]D. T. Cromer and J. B. Mann, Acta Crystallogr. Sect. A 24, 321 (1968).
[17]C. C. McBride, J. W. Spretnak, and R. Speiser, Trans. Am. Soc. Met. 46, 499 (1954).
[18]D. K. Brown, I. Nowik, and D. I. Paul, Solid State Commun. 24, 711 (1977).
[19]P. J. Schurer and A. H. Morrish, J. Magn. Magn. Mater. 15-18, 577 (1980).
[20]P. J. Schurer and A. H. Morrish, Phys. Rev. B 20, 4660 (1979).
[21]C. L. Chien and R. Hasegawa, Phys. Rev. B 16, 3024 (1977).